Ab Initio Study of the Cyclooctatetraenyl Radical

Maria G. Moreno-Armenta[†,‡] and Andrew L. Cooksy*[,†,§]

Department of Chemistry, San Diego State University, San Diego, California 92182-1030, Centro de Ciencias de la Materia Condensada, Universidad Nacional Autónoma de México, Apartado Postal 2681, Ensenada Baja California, 22800, México, and Centro de Graduados e Investigacion del Instituto Tecnológico de Tijuana, Apdo Postal 1166, Tijuana, Baja California, México

Received: August 6, 2004; In Final Form: February 24, 2005

Ab initio calculations have been carried out on the 1,3,5,7- and 1,2,4,7-tetraene configurations of the cyclooctatetraenyl radical at UHF, ROHF, MCSCF, ROCISD, QCISD, and CCSD(T) levels of theory with 6-311G(d,p) and cc-pVDZ basis sets. Although spin contamination is present, the ROCISD calculations support the energies obtained from less intensive, UHF-based coupled cluster calculations over the energies obtained from MCSCF analysis of the π-electron orbitals. The 1,3,5,7-form is a local minimum at the coupled cluster levels, higher in energy than the resonance-stabilized 1,2,4,7-form by 10−13 kJ/mol, but bounded by a barrier of less than 0.5 kJ/mol. The isomerization surface connecting these two structures is described and results reported from integration of the vibrational Schrödinger equation on that surface. Excited vibrational states at energies just above the isomerization barrier are dominated by the character of the 1,3,5,7-tetraenyl radical, which suggests that chemistry involving this intermediate at typical combustion temperatures may branch at this juncture.

Introduction

The cyclooctatetraenyl radical has attracted recent attention as an intermediate in the complex combustion chemistry of unsaturated hydrocarbons. Considerable research has been conducted on benzene and phenyl radical formation mechanisms,[1−12] and investigations are now broaching the intermediates formed from subsequent reactions of the aromatic species. The C_8H_7 radical is encountered among reactions of acetylene with many radicals, modeled computationally by Wang and Frenklach using the AM1 method.[13] They calculated the RRKM reaction rate coefficients, correcting the AM1 molecular parameters to reproduce the available experimental data. Richter et al.[9] carried out a theoretical study of acetylene addition to phenyl and 1-naphthyl radicals. The potential energy surfaces (PES) of the reactions, including local minima and transition states were explored with use of BLYP and B3LYP density functional theory. Moriarty et al.[14] investigated the migration of hydrogen in the phenylethen-2-yl radical by determining optimal geometries and reaction energies using many levels of quantum theory coupled with RRKM theory to calculate rate coefficients and equilibrium constants. They suggest that the hydrogen migration could be regarded as an additional route to aromatic ring growth and ring fragmentation.

More recently the mechanism of the $C_6H_5 + C_2H_2$ reaction has been investigated by Tokmakov and Lin[15] using various quantum chemical methods. In that study they report several isomerization pathways from the initially formed, chemically activated $C_6H_5C_2H_2$ to produce phenylacetylene, benzocyclobutadiene, and pentalene. Zero-point-corrected energies relative to $C_6H_5 + C_2H_2$ were calculated by the [G2M-(RCC6,RMP2)] and G2M(RCC5,RMP2) methods.

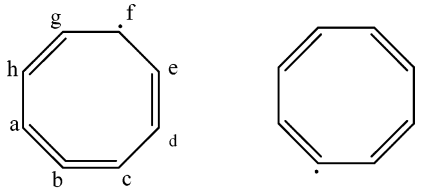

I II

Figure 1. Canonical structures for the cyclooctatetraenyl radical.

Tokmakov and Lin's work focused on the minimum energy paths connecting distinct structural isomers, and did not investigate alternative chemistries of the intermediates and how these might be affected by thermal excitation. The intermediate monocyclic C_8H_7 radical, cyclooctatetraenyl, is similar to other unsaturated, π-conjugated radicals studied in our research group[16−18] in that two favorable, nonequivalent canonical structures may be drawn (Figure 1). Because these geometries differ in carbon orbital hybridizations, the geometries may differ enough that a potential energy barrier separates them into observably distinct isomers. On the other hand, if the relative stabilities are also very different, the potential energy surface is more likely to slope gradually from the less stable to the more stable structure, with no intervening barrier. In this case, the distinction is between the 1,2-diene form of the radical **I** and the 1,3,5,7-tetraenyl radical **II**, the latter being the daughter radical in the image of the famously antiaromatic 1,3,5,7-cyclooctatetraene. If the radical is formed by hydrogen abstraction from cyclooctatetraene, the isomerization from **I** to **II** exchanges sp^2 character at the site of the abstraction (atom b) for sp character, pushing the spin density of the unpaired electron to the opposite end of the ring. Although the twisting of the CCH planes at either end of the allene group would significantly strain a smaller ring, the 1,2-diene **I** is in fact significantly

* To whom correspondence should be addressed at San Diego State University. Phone: 619-594-5571. Fax: 619-594-4634. E-mail: acooksy@sciences.sdsu.edu.

† San Diego State University.

‡ Universidad Nacional Autónoma de México.

§ Centro de Graduados e Investigacion del Instituto Tecnológico de Tijuana.

10.1021/jp046460m CCC: $30.25
Published on Web 03/30/2005

favored by the delocalization of the unpaired electron across the remaining five carbon atoms. Structure **I** is the configuration appearing in Tokmakov and Lin's study.[15] In this paper we present ab initio properties of the electronic and vibrational wave functions of the cyclooctatetraenyl radical in its two configurations, and estimate the relevance of this isomerization to the subsequent addition chemistry of the radical.

Methods

Initial geometry optimizations were carried out from canonical geometries for structures **I** and **II** under the unrestricted Hartree−Fock (UHF) and restricted open shell Hartree−Fock (ROHF) approximations, using the small 3-21G split-valence basis set. Geometries were subsequently improved at the larger 6-311G(d,p)[19,20] and cc-pVDZ basis sets,[21] which each contain d-type polarization functions on the carbons and p-type polarization functions on the hydrogens. Higher level calculations were carried out with the cc-pVDZ basis, which employs fewer functions than 6-311G(d,p) but has been of equal quality in similar investigations.[18] The structures were re-optimized at the QCISD level, effectively a coupled-cluster method that includes single and double excitations from a single UHF reference in estimating the correlation energy.[22,23] Because the spin contamination of the UHF reference is large, the qualitative conclusions of the QCISD calculations were tested by optimizations at the RHF-based MCSCF level, followed by single-point calculations at the MCSCF geometries using a second-order CI expansion of the ROHF wave functions (ROCISD).[24] The MCSCF used an active space of 9 electrons in 9 orbitals, covering the π bonding/antibonding system and the singly occupied orbital. The ROCISD incorporated single and double excitations of the electrons from all 20 valence orbitals into the lowest 28 unoccupied orbitals, resulting in wave functions composed of 2.5 million configuration space functions. As the orbitals in the ROCISD active space encompass less than 25% of all the virtual orbitals obtained from the cc-pVDZ basis, the ROCISD results are not expected to be fully converged. The final quoted geometries and vibrational frequencies given here were determined at the QCISD/cc-pVDZ level. We note that this level has been adequate in previous studies where direct comparison to experimental data is available, predicting for example the relative formation enthalpies of a diverse set of C_4H_5 isomers to within 5 kJ/mol.[18] The transition state between **I** and **II** was optimized at the QCISD/cc-pVDZ level after refining the initial geometry by carrying out a relaxed potential energy scan, varying the $C_aC_bC_c$ angle from 140° to 162.5° and the bond distance C_bC_c from 1.30 to 1.42 Å. That the structure is a transition state was confirmed by the single imaginary constant in the harmonic frequency analysis. Single-point energies were calculated at the coupled-cluster CCSD(T)/cc-pVDZ level, which incorporates an estimated contribution from triple excitations.[25−27] All electronic structure calculations in this work were performed with the Gaussian 03[28] and Gamess codes[29] on Compaq DS-10, Intel PIII and Xeon, and AMD Opteron computer systems. Visualization of the results was accomplished with Molekel.[30]

In the relaxed, two-dimensional scan of the QCISD/cc-pVDZ surface, 46 partially optimized geometries were obtained. Although these 46 points should be sufficient to convey an accurate picture of the PES in the region of the two minima, study of the excited state vibrational wave functions requires sampling along these coordinates at much higher resolution. To artificially increase the resolution of the PES scan for integration, the value of a parameter p at any point r (the C_bC_c bond length) and θ (the $C_aC_bC_c$ bond angle) was estimated according to:

$$p(r,\theta) = \frac{1}{\sum_{i=1}^{N}\sum_{j=1}^{N} w_i w_j} \sum_{i=1}^{N}\sum_{j=1}^{N}\left[p_i + \frac{(p_j - p_i)(r - r_i)(\theta - \theta_i)}{\sqrt{\sigma_r \sigma_\theta}|(r_j - r_i)(\theta_j - \theta_i)|}\right] w_i w_j \quad (1)$$

where the weighting factors are given by

$$w_i = \exp[-2(r - r_i)^2/(\sigma_t \sigma_r)] \exp[-2(\theta - \theta_i)^2/(\sigma_t \sigma_\theta)] \quad (2)$$

If we label the point of interpolation r,θ by k, this interpolation scheme estimates a value of p based on two criteria: how close k is to any given points i and j, and how close k is to lying on the straight line connecting i and j in the parameter space of r and θ. The value σ_t scales the argument of the Gaussian weighting factors such that large values of σ_t make distant geometries i less likely to influence the value of p at point k. The values σ_r and σ_θ are the variances in the coordinate values of r and θ that appear in the interpolated grid; they scale the impact of each coordinate so that, for example, the units chosen do not affect the weighting. When selected optimized geometries were excluded from the input, this scheme with a value of 0.1 for σ_t predicted the correct potential energy at those r,θ values to within 5%, and values of the variable internal coordinates were predicted to within 2%. Similar results were obtained in an earlier test run (as part of this work) on the formyl radical. The remaining error can always be further reduced with greater sampling of the PES.

By this method, an effective vibrational potential energy surface was constructed on a 400 × 400 point square grid at resolutions of 0.0008 Å in r and 0.14° in θ. Similarly, the kinetic energy contribution to the vibrational Hamiltonian was discretized on this surface by estimating interpolated geometries at each point on the grid. The molecular structure is a function of 39 internal coordinates (bond lengths, angles, and dihedrals), and the values of each coordinate were computed at each point r,θ by eq 1 to obtain a geometry for that point. The resulting geometry was converted to Cartesian coordinates, so that the kinetic energy operator could remain in Cartesian form. Finally, the moment of inertia tensor was diagonalized to prevent rotations and center-of-mass translations from contributing to the kinetic energy.

Integration of the vibrational Schrödinger equation was carried out on this grid, by using numerical derivatives of the atomic displacements among the grid geometries to estimate the kinetic energy integrals. The ground vibrational state was optimized variationally as a linear combination of two-dimensional harmonic oscillator wave functions, using an adjustable set of four variables: the centers (r_0 and θ_0) and effective force constants (k_r and k_θ) along each dimension. Convergence of the energies to within 10^{-3} was established for the states discussed below as a function of the grid size and number of basis functions. Excited-state wave functions and energies were approximated by the higher energy eigenstates of the Hamiltonian matrix.

Results and Discussion

At the UHF level, only a single planar geometry is found for the cyclooctatetraenyl radical, but the expectation value of the spin squared operator $\langle S^2 \rangle$ at that geometry is 2.41, making these calculations highly suspect. However, at other levels of theory, the geometries near both configurations are both minima on

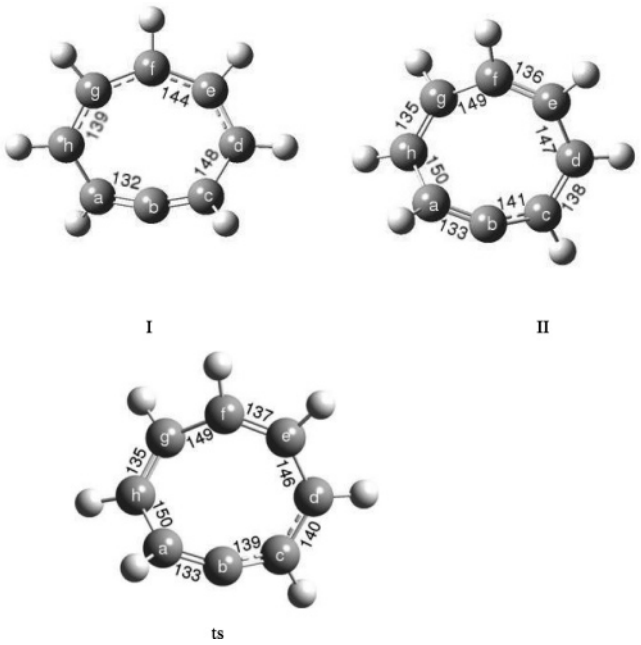

Figure 2. QCISD/cc-pVDZ optimized geometries for **I** and **II** and the transition state (**ts**), with bond lengths given in pm.

the PES. At these nonplanar geometries, the energy separation among the π molecular orbitals expands significantly, raising the energy of the quartet state responsible for most of the spin contamination in the UHF calculations. The UHF $\langle S^2 \rangle$ values drop to 1.75−1.85 for these stationary points. Although immune from spin-contamination, the ROHF and MCSCF calculations predict configuration **II** is more stable than configuration **I** by 28.8 and 2.2 kJ/mol, respectively. This nonintuitive result is not supported by the ROCISD calculations, however, which find **I** more stable than **II** by 7.3 kJ/mol, in fair agreement with QCISD and CCSD(T). The enhanced stability of **II** in the ROHF and MCSCF results would be a logical consequence of the tendency of ROHF wave functions to localize the electron distribution too strongly in conjugated systems. Evidence of the need for dynamic correlation corrections to MCSCF wave functions was extensively documented in studies of the Cope rearrangement and other pericyclic reactions by Houk,[31] Davidson,[32] and Borden[33] (see also references therein). In those studies it is found that MCSCF alone tends to overemphasize localized diradical character in the transition states, when experimental evidence indicates more aromaticity. The calculated MCSCF wave functions in our work have less than 0.5% character from triple and higher substitutions, indicating that a complete active space CI is not necessary, and the ROCISD calculations are able to capture an additional 15 mhar/carbon of the correlation energy. For these reasons, we expect the ROCISD to be more reliable than the MCSCF. Unfortunately, the computational intensity of the individual ROCISD calculations and the lack of analytic gradients for geometry optimizations and frequency analysis make it an impractical method at present for describing general features of the PES. The remaining discussion therefore relies on the QCISD and CCSD(T) results.

The optimized QCISD/cc-pVDZ geometries are shown with bond length values in Figure 2. Although all the calculations were symmetry unconstrained, the geometry of configuration **I** has C_2 symmetry, with the symmetry axis passing through atoms b and f in Figure 1. Configuration **I** is characterized by a $C_aC_bC_c$ angle approaching linearity (162.5°), with the bonds C_aC_b and C_bC_c having typical double bond lengths of 1.323 Å. The dihedral angles give the overall cycle a biplanar geometry:

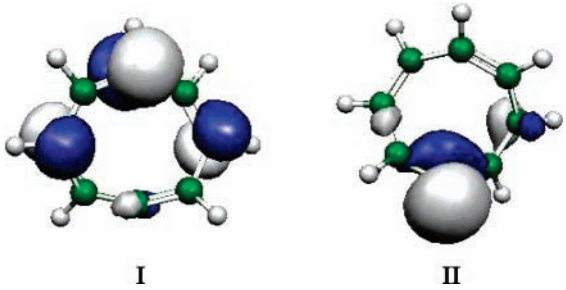

Figure 3. The singly occupied ROHF molecular orbitals. The molecular orientations are the same as in Figure 2.

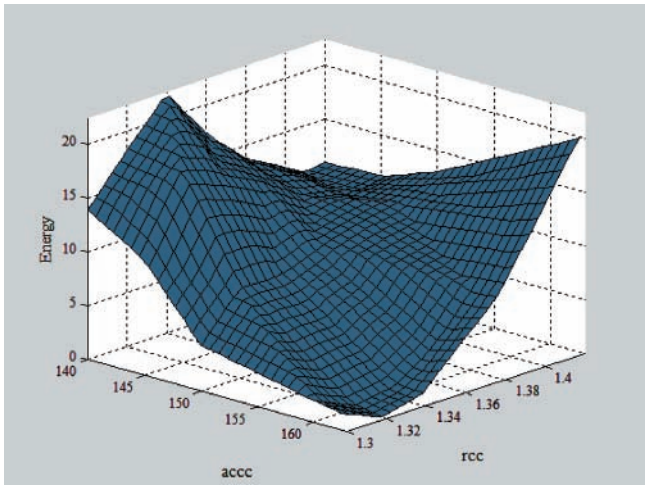

Figure 4. Selected region of the QCISD/cc-pVDZ potential energy surface as a function of the $C_aC_bC_c$ bend angle (accc) and C_bC_c bond length (rcc). Configuration **I** lies in the forward area and configuration **II** lies to the rear in this plot.

atoms d−h in Figure 1 are roughly coplanar, while the plane of atoms a−c differs by a 32° rotation about the symmetry axis. The dihedral angles $C_dC_eC_fC_g$ and $C_eC_fC_gC_h$ are actually 18°, similar to the 15° dihedrals calculated for the EE conformer of the pentadienyl radical at the same level of theory.[34] As shown in Figure 3, the unpaired electron is delocalized across the π-system of atoms e−h in Figure 1, but peaks near atom f. The geometry reported by Tokmakov and Lin in their ab initio calculations is consistent with configuration **I**.

In contrast, configuration **II** has no point group symmetry, with alternating single and double CC bond lengths, and the unpaired electron is almost completely localized in an sp^2-character orbital on atom C_b. The $C_aC_bC_c$ angle is 143.3°, indicating that the sp^2 character of the orbitals is distributed toward substantial s-character in the CC bonds and correspondingly greater p-character in the unpaired electron orbital.

The QCISD and CCSD(T) calculations find configuration **I** to be more stable than **II**. The difference in energies between **I** and **II** is calculated to be 10.7 kJ/mol at QCISD and 12.4 kJ/mol at CCSD(T). The coupled cluster levels have repeatedly proven themselves more accurate than MCSCF in systems with comparable spin contamination,[18,35] and the remaining discussion rests on those calculations.

The isomerization potential is rather flat and the second minimum is shallow, as illustrated in Figure 4. The isomerization energy is 10.67 kJ/mol, whereas the barrier relative to the global minimum is 10.98 kJ/mol. The transition state lies only 0.3 kJ/mol or 25 cm^{-1} above configuration **II**, scarcely enough to isolate from each other the vibrational wave functions corresponding to the two structures. Consequently, the geometry of the transition state, as shown in Figure 2, closely resembles that

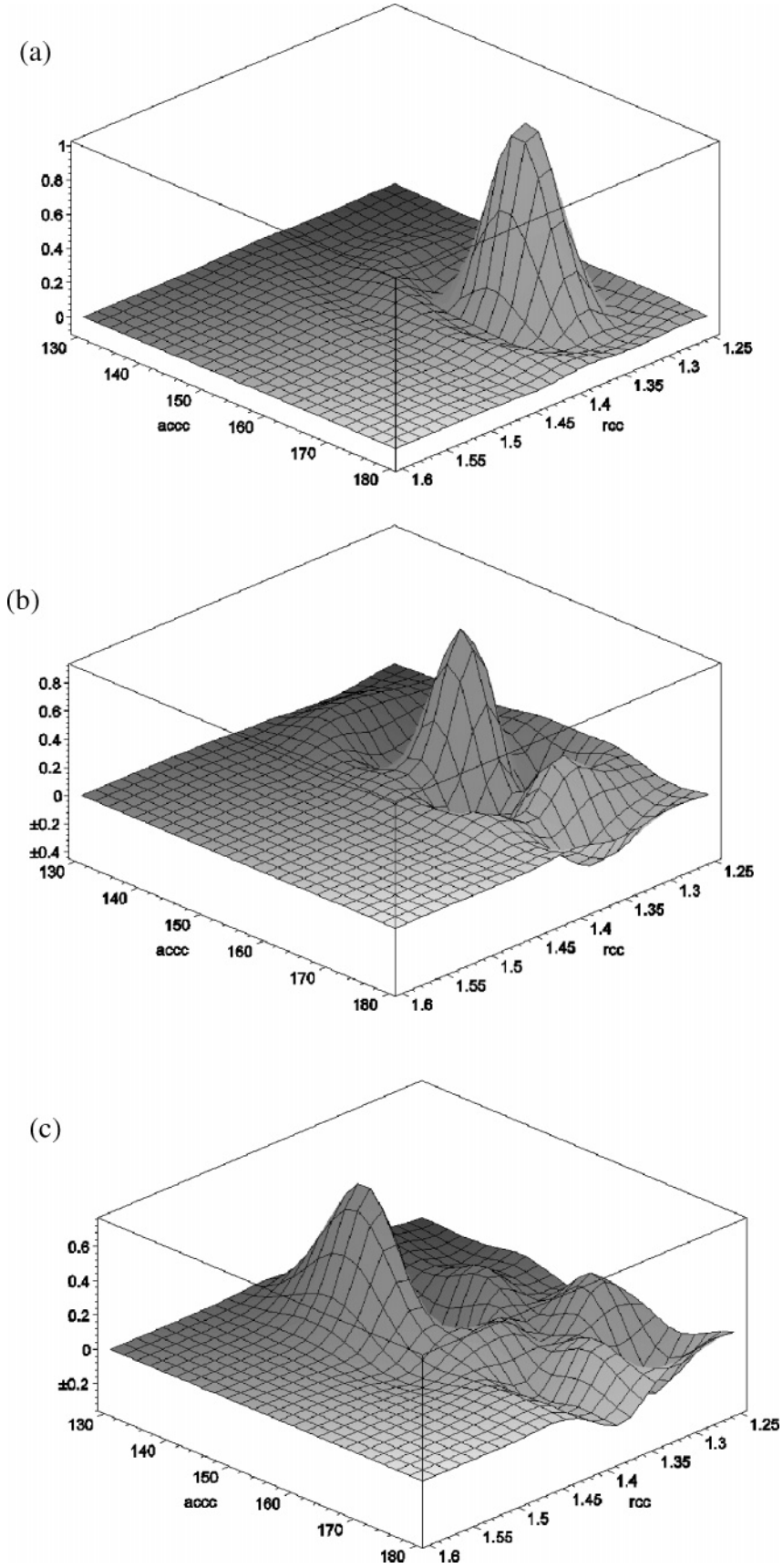

Figure 5. Predicted vibrational wave functions as functions of the $C_aC_bC_c$ bend angle (accc) and C_bC_c bond length (rcc) for the states (a) $v = 0$ at 124 cm^{-1}, (b) $v = 6$ at 501 cm^{-1}, and (c) $v = 13$ at 892 cm^{-1}.

of **II**. However, the barrier height relative to **I** corresponds to a temperature of about 1500 K, suggesting that the region of the potential surface corresponding to **II** is accessible in the combustion systems where this chemistry occurs.

In the transition state, the normal mode with imaginary harmonic frequency, 126i cm^{-1}, couples the many local parameter changes inherent in transforming the sp^2 center b in **I** to sp in **II**: bending the $C_aC_bC_c$ angle, lengthening the C_bC_c

bond, and adjusting dihedrals to change the biplanar form of **I** to the boatlike **II** conformation. This latter, relatively large-amplitude local motion dominates the kinetic energy term in the solution to the vibrational Schrödinger equation along the **I**−**II** isomerization coordinate. Consequently, the lowest predicted vibrational constants from the harmonic analysis follow the isomerization coordinate. However, for our anharmonic vibrational analysis, we parametrized the PES using the $C_aC_bC_c$ angle and C_bC_c length rather than the dihedrals. This was partly to examine the vibrational wave function in terms of the parameters more closely associated with the change in MO hybridization at atom b, but also because a relaxed PES scan of the dihedrals tends to follow lower energy conformational isomerization paths rather than the configurational change intended for mapping. The resulting energies and wave functions from our analysis should be qualitatively accurate for excitation along the isomerization coordinate. The neglect of so many anharmonic couplings among the normal modes (given that at least three local modes are complicit in the isomerization) makes quantitative precision unlikely, even if the PES were assumed to be flawless. What this analysis does offer is an association between the degree of thermal excitation in the system and the ensuing structural effects. In the vibrational ground state (Figure 5a), the radical is localized near canonical structure **I**, although with considerable zero-point $C_aC_bC_c$ bending. The lowest lying vibrational states on this surface correspond approximately to excitation of that bend (Figure 5b), with the classically allowed region increasing rather slowly with excitation. For geometries in this region, the spin density is still delocalized across atoms d, f, and h in Figure 1. However, once the energy reaches the isomerization barrier, the parameter space of configuration **II** becomes accessible and the classically allowed region of vibration increases sharply. The first vibrational state above this energy (Figure 5c) has substantial amplitude in the previously unavailable region of **II**, forming an effective isomeric state of **II** with the spin strongly localized on atom b. This effect is a predictable result of the anomalous potential surface for this and similar relocalization problems.[36] If vibrational states at energies above the isomerization barrier sampled **I** and **II** equally, temperatures exceeding 1500 K would excite at least 20% of the cyclooctatetraenyl radicals to structure **II**. This predicts, for example, that termination reactions involving hydrogen addition will produce the parent 1,3,5,7-tetraene at greater rates than if only the more stable **I** were present, because the average spin density at atom b increases with the population of **II**.

Conclusions

Two minimum energy geometries are identified for the cyclooctatetraenyl radical by QCISD/cc-pVDZ calculations. The less stable geometry nominally has the electron distribution of the parent 1,3,5,7-cyclooctatetraene, and is separated by a very low 0.3 kJ/mol barrier from the 1,2-dienyl radical 10−13 kJ/mol lower. Although the predicted barrier between the two structures is too weak to allow for a bound vibrational state corresponding solely to isomer **II**, the relative energy of the second structure is low enough that it may represent a significant fraction of the molecular geometries sampled at combustion temperatures. Given the distinct spin localizations of the two structures, the chemistry of high-temperature systems involving the cyclooctatetraenyl radical may branch in different directions after the formation of this intermediate.

Acknowledgment. Financial support was provided through NSF Grant CHE-0216563, Proyect DGAPA IN-104803-3 (Mexico), and the Blasker Fund of the San Diego Foundation. M.G.M. acknowledges support from DGAPA for her postdoctoral study.

Supporting Information Available: Optimized geometries, $\langle S^2 \rangle$ values, harmonic vibrational frequencies, and zero-point energies for stationary point calculations. This material is available free of charge via the Internet at http://pubs.acs.org.

References and Notes

(1) Bockhorn, H.; Fetting, F.; Wenz, W. *Ber. Bunsen-Ges Phys. Chem.* **1983**, *87*, 1073.
(2) Wang, H.; Frenklach, M. *Combust. Flame* **1997**, *110*, 173.
(3) Westmoreland, P. R.; Dean, A. M.; Howard, J. B.; Longwell, J. P. *J. Phys. Chem.* **1989**, *93*, 8171.
(4) Kazakov, A.; Wang, H.; Frenklach, M. *Combust. Flame* **1995**, *100*, 111.
(5) Richter, H.; Mazyar, O. A.; Sumathi, R.; Green, W. H.; Howard, J. B.; Bozzelli, J. W. *J. Phys. Chem. A* **2001**, *105*, 1561.
(6) Marinov, N. M.; Pitz, W. J.; Westbrook, C. K.; Vincitore, A. M.; Castaldi, M. J.; Senkan, S. M. *Combust. Flame* **1998**, *114*, 192.
(7) Skjøth-Rasmussen, M. S.; Glarborg, P.; Østberg, M.; Johannessen, J. T.; Livbjerg, H.; Jensen, A. D.; Christensen, T. S. *Combust. Flame* **2004**, *136*, 91.
(8) Frenklach, M. *Phys. Chem. Chem. Phys.* **2002**, *4*, 2028.
(9) Richter, H.; Howard, J. B. *Phys. Chem. Chem. Phys.* **2002**, *4*, 2038.
(10) Richter, H.; Howard, J. B. *Prog. Energy Combust. Sci.* **2000**, *26*, 565.
(11) Kennedy, I. M. *Prog. Energy Combust. Sci.* **1997**, *23*, 95.
(12) McEnally, C. S.; Pfefferle, L. D. *Combust. Flame* **2004**, *136*, 155.
(13) Wang, H.; Frenklach, M. *J. Phys. Chem.* **1994**, *98*, 11465.
(14) Moriarty, N. W.; Brown, N. J.; Frenklach, M. *J. Phys. Chem. A* **1999**, *103*, 7127.
(15) Tokmakov, I. V.; Lin, M. C. *J. Am. Chem. Soc.* **2003**, *125*, 11397.
(16) Cooksy, A. L.; Tao, F.-M.; Klemperer, W.; Thaddeus, P. *J. Phys. Chem.* **1995**, *99*, 11095.
(17) Cooksy, A. L. *J. Phys. Chem* **1998**, *102*, 5092.
(18) Parker, C. L.; Cooksy, A. L. *J. Phys. Chem. A* **1999**, *103*, 2160.
(19) Krishnan, R.; Binkley, J. S.; Seeger, R.; Pople, J. A. *J. Chem. Phys.* **1980**, *72*, 650.
(20) Frisch, M. J.; Pople, J. A.; Binkley, J. S. *J. Chem. Phys.* **1984**, *80*, 3265.
(21) Dunning, T. H. *J. Chem. Phys.* **1989**, *90*, 1007.
(22) Pople, J. A.; Head-Gordon, M.; Raghavachari, K. *J. Chem. Phys.* **1987**, *87*, 5968.
(23) Pople, J. A.; Head-Gordon, M.; Raghavachari, K. *J. Chem. Phys.***1989**, *90*, 4635.
(24) Shepard, R. *Adv. Chem. Phys.* **1987**, *69*, 63.
(25) Noga, J.; Bartlett, R. J. *J. Chem. Phys.* **1987**, *86*, 7041.
(26) Urban, M.; Noga J.; Cole, S. J.; Bartlett, R. *J. Chem. Phys.* **1985**, *83*, 4041.
(27) Raghavachari, K.; Trucks, G. W.; Pople, J. A.; Head-Gordon, M. *Chem. Phys. Lett.* **1989**, *157*, 479.
(28) Frisch, M. J.; Trucks, G. W.; Schlegel, H. B.; Scuseria, G. E.; Robb, M. A.; Cheeseman, J. R.; Montgomery, J. A., Jr.; Vreven, T.; Kudin, K. N.; Burant, J. C.; Millam, J. M.; Iyengar, S. S.; Tomasi, J.; Barone, V.; Mennucci, B.; Cossi, M.; Scalmani, G.; Rega, N.; Petersson, G. A.; Nakatsuji, H.; Hada, M.; Ehara, M.; Toyota, K.; Fukuda, R.; Hasegawa, J.; Ishida, M.; Nakajima, T.; Honda, Y.; Kitao, O.; Nakai, H.; Klene, M.; Li, X.; Knox, J. E.; Hratchian, H. P.; Cross, J. B.; Adamo, C.; Jaramillo, J.; Gomperts, R.; Stratmann, R. E.; Yazyev, O.; Austin, A. J.; Cammi, R.; Pomelli, C.; Ochterski, J. W.; Ayala, P. Y.; Morokuma, K.; Voth G. A.; Salvador, P.; Dannenberg, J. J.; Zakrzewski, V. G.; Dapprich, S.; Daniels, A. D.; Strain, M. C.; Farkas, O.; Malick, D. K.; Rabuck, A. D.; Raghavachari, K.; Foresman, J. B.; Ortiz, J. V.; Cui, Q.; Baboul, A. G.; Clifford, S.; Cioslowski, J.; Stefanov, B. B.; Liu, G.; Liashenko, A.; Piskorz, P.; Komaromi, I.; Martin, R. L.; Fox, D. J.; Keith, T.; Al-Laham, M. A.; Peng, C. Y.; Nanayakkara, A.; Challacombe, M.; Gill, P. M. W.; Johnson, B.; Chen, W.; Wong, M. W.; Gonzalez, C.; Pople, J. A. *Gaussian 03*, Revision A.1; Gaussian, Inc.: Pittsburgh, PA, 2003.
(29) Schmidt, M. W.; Baldridge, K. K.; Boatz, J. A.; Elbert, S. T.; Gordon, M. S.; Jensen, J. H.; Koseki, S.; Matsunaga, N.; Nguyen, K. A.; Su, S. J.; Windus, T. L.; Dupuis, M.; Montgomery, J. A. *J. Comput. Chem.* **1993**, *14*, 1347.
(30) Portmann, S.; Lüthi, H. P. *CHIMIA* **2000**, *54*, 766.
(31) Li, Y.; Houk, K. N. *J. Am. Chem. Soc.* **1993**, *115*, 7478.
(32) Kozlowski, P. M.; Dupuis, M.; Davidson, E. R. *J. Am. Chem. Soc.* **1995**, *117*, 774.
(33) Borden, W. T.; Davidson, E. R. *Acc. Chem. Res.* **1996**, *29*, 67.
(34) Martinez, C.; Cooksy, A. L. *J. Org. Chem.* **2002**, *67*, 2295.
(35) Cooksy, A. L. *J. Am. Chem. Soc.* **2001**, *123*, 4003.
(36) Cooksy, A. L. *J. Am. Chem. Soc.* **1995**, *117*, 1098.